Effects of Phonon Scattering on Discrete-Impurity-Induced Current Fluctuation in Silicon Nanowire Transistors

Nobuya Mori[†], Masashi Uematsu[*†], Gennady Mil'nikov[†], Hideki Minari[†], and Kohei M. Itoh[*†]
Graduate School of Engineering, Osaka University, Osaka 565-0871, Japan
[*]School of Fundamental Science and Technology, Keio University, Yokohama 223-8522, Japan
[†]CREST, Japan Science and Technology Agency (JST), Tokyo 102-0076, Japan
Email: nobuya.mori@eei.eng.osaka-u.ac.jp

***Abstract*—Effects of phonon scattering on random-dopant-induced current fluctuations are investigated in silicon nanowire transistors. Active dopant distributions obtained through kinetic Monte Carlo simulation are introduced into 10 nm-gate-length n-type nanowire transistors, and the current-voltage characteristics are calculated by the non-equilibrium Green's function method. The current fluctuation is found to be suppressed by ~40 % by phonon scatterings at the on-state, while it is very weakly affected at the off-state.**

I. Introduction

The gate length, L_g, of metal-oxide-semiconductor field-effect-transistors (MOSFETs) has been scaled down to below 30 nm. At this scale, the channel length is comparable to the electron mean free path, and electrons may be scattered in the channel region only a few times. In such a situation, it is not well understood how scattering affects the transport characteristics. Energy dissipation through electron-phonon scattering should also be inevitable in irreversible electron transport. In addition, it is pointed out that fluctuation of device characteristics due to random discrete dopant (RDD) distribution becomes major concern for nanoscale transistors [1]–[5]. Effects of the RDD distribution are usually analyzed with a randomly generated dopant distribution. The actual RDD distribution, however, should be correlated with the process condition, and can be different from a mathematically generated one. In our previous study [6], [7], we investigated the effects of RDD on characteristics of gate-all-around (GAA) silicon nanowire (Si NW) transistors using a kinetic Monte Carlo (KMC) simulator for generating distribution of active dopant atoms and the non-equilibrium Green's function (NEGF) method for calculating the current-voltage characteristics under the condition of neglecting phonon scattering. In the present study, we investigate the effects of phonon scattering on the RDD-induced current variability in Si NW transistors.

II. Calculation Method

A. Random Dopant Distribution

Discrete random arsenic (As) distributions in Si NWs are obtained using the Sentaurus KMC simulator [8]. Si NWs (3 nm wide, 3 nm high, and 30 nm long) covered with 1 nm-thick SiO_2 and with a thick mask are implanted with As (0.5 keV, 2×10^{14} cm^{-2}) and annealed at 1000 °C with a hold time of 0 s [Fig. 1(a)]. We introduce side-wall gate spaces of 2 nm thickness to reduce the V_{th} fluctuation [7], [9]. We

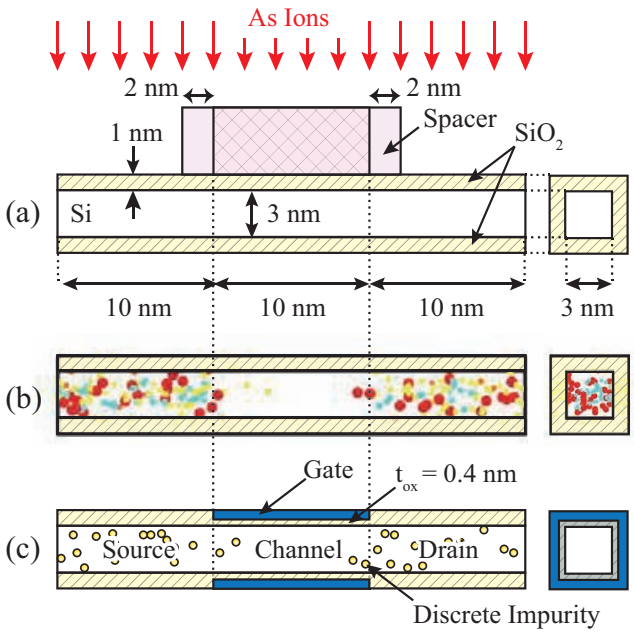

Fig. 1. (a) KMC simulation. (b) Discrete As distribution in the Si NW. Red dots show active As atoms in Si, light blue As clusters, orange As at the oxide/Si interface, and yellow As in the oxide. (c) Device structure for NEGF calculation.

investigate statistical variations using different discrete As distributions [Fig. 1(b)] generated with different random seeds. We find that ~30 % of As atoms implanted into the Si region are active in the Si NW and others are in As clusters (~35 %), at the oxide/Si interface (~10 %), and in the oxide (~25 %). The As clusters are inactive and immobile in Si.

B. Current-Voltage Characteristics

The active As distributions obtained through the KMC simulation are introduced into n-type GAA Si NW MOSFETs, whose device structure is given in Fig. 1(c). The drain-current–gate-voltage (I_d–V_g) characteristics are calculated by the NEGF method with an effective mass approximation [10]–[13]. The conduction band is expressed in terms of six elliptic valleys with the bulk effective masses. The coupled eigen-mode expansion method [14], [15] is adopted for solving the NEGF transport equation. To accelerate the convergence of the iterative solution, we adopt the Anderson mixing [16] and the

978-1-4673-5736-4/13/$31.00 ©2013 IEEE

Newton method [17]. The discrete impurities are treated with a cloud-in-cell charge assignment scheme [18]. We include phonon scattering within the self-consistent Born approximation [10], [11] assuming constant deformation potentials for g-type and f-type phonons and an elastic approximation for acoustic phonons [19]. For g-type and f-type phonons, the in/out-scattering functions [10] can be written as

$$\Sigma_{\rm ph}^{\rm in/out}(\lambda,\lambda';E) = \sum_{\nu,\boldsymbol{q}}\sum_{\lambda_1,\lambda_2} |U_\nu|^2 \langle\lambda|e^{i\boldsymbol{q}\cdot\boldsymbol{r}}|\lambda_1\rangle\langle\lambda_2|e^{-i\boldsymbol{q}\cdot\boldsymbol{r}}|\lambda'\rangle \times\Big[N_\nu G^{\rm n/p}(\lambda_1,\lambda_2;E\mp\hbar\omega_\nu) + (N_\nu+1)\,G^{\rm n/p}(\lambda_1,\lambda_2;E\pm\hbar\omega_\nu)\Big], \quad (1)$$

where λ specifies the basis states of electrons, ν denotes the phonon modes, $\hbar\omega_\nu$ is the phonon energy, $N_\nu = 1/[\exp(\hbar\omega_\nu/kT) - 1]$, U_ν is the interaction potential, and $G^{n/p}$ are the correlation functions. For acoustic phonons, the in/out-scattering functions can be written in a similar form in the equipartition approximation. We use the bulk phonon-scattering parameters in Refs. [20] and [21]. Phonon confinement effects [22] and inelasticity of acoustic phonon scattering [23] are neglected.

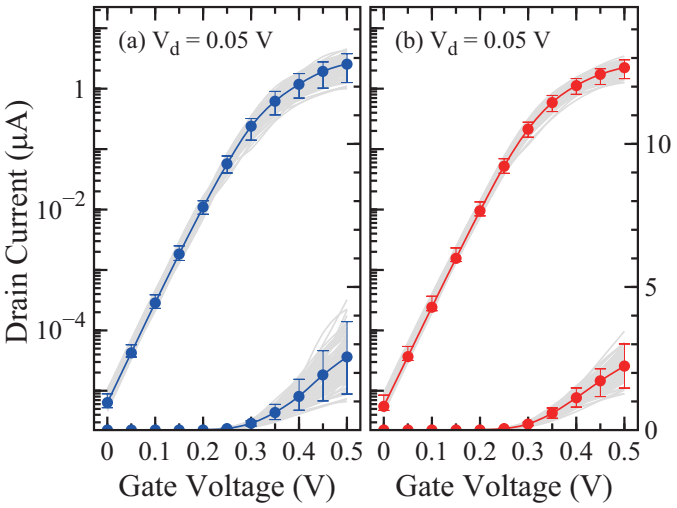

Fig. 2. I_d–V_g characteristics without phonon scattering (a) and those with it (b) at V_d = 0.05 V. Gray lines show the I_d–V_g of 100 samples with different discrete As distributions. Close circles show the median ($I_{50\%}$). The upper error bars represent 95 percentile while the lower error bars represent 5 percentile values ($I_{95\%}$ and $I_{5\%}$).

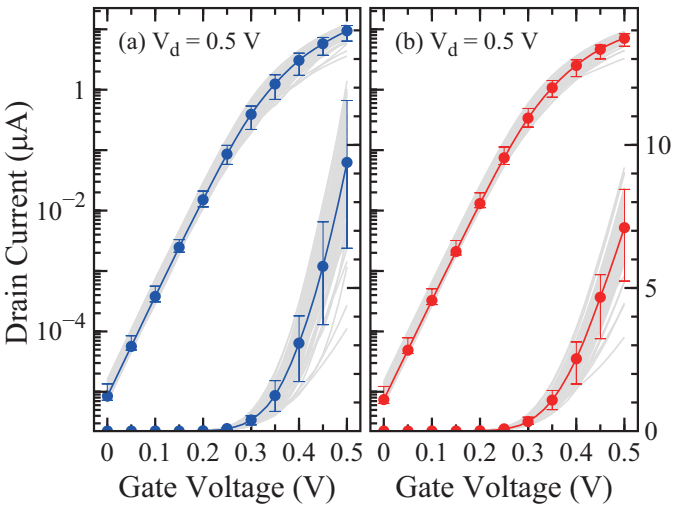

Fig. 3. The same as Fig. 2 but for V_d = 0.5 V.

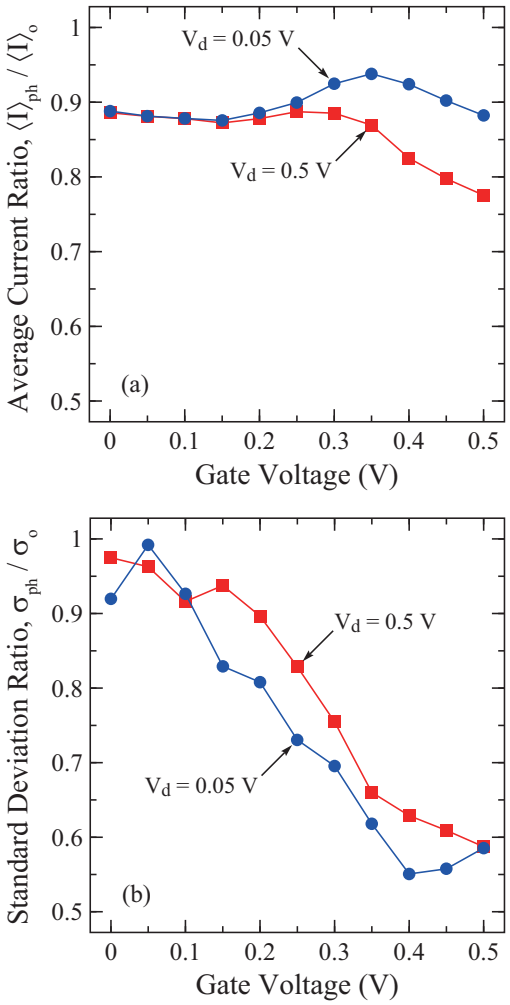

Fig. 4. (a) V_g-dependence of $\langle I\rangle_{ph}/\langle I\rangle_o$, where $\langle I\rangle_{ph}$ ($\langle I\rangle_o$) is the average current with (without) phonon scattering. (b) Standard deviation ratio, σ_{ph}/σ_o, as a function of V_g, where σ_{ph} (σ_o) is the standard deviation of the current values with (without) phonon scattering.

III. Results and Discussion

A. Current-Voltage Characteristics

Figures 2 and 3 show calculated I_d–V_g characteristics at V_d = 0.05 and 0.5 V, respectively. We have simulated 100 samples with different discrete As distributions (gray lines). The close circles show the median ($I_{50\%}$). The upper error bars represent 95 percentile while the lower error bars represent 5 percentile values ($I_{95\%}$ and $I_{5\%}$). The average number of dopants in the source or drain expansion is ~ 15, which corresponds to ~ 1.7×10^{20} cm^{-3}, while the average number of dopants in the channel region is ~ 0.5. Since the spacers of 2 nm thickness reduce the penetration of dopants deep into the channel region, the threshold-voltage variations are greatly suppressed [7], [9].

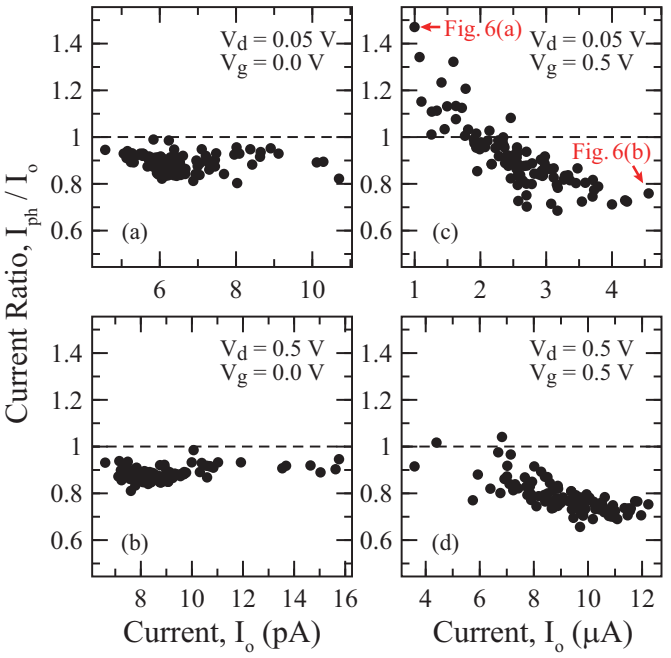

Fig. 5. Correlation between I_{ph}/I_o and I_o at the off-state [(a) and (b)] and at the on-state [(c) and (d)]. Here I_{ph} (I_o) is the current value of an individual sample with (without) phonon scattering.

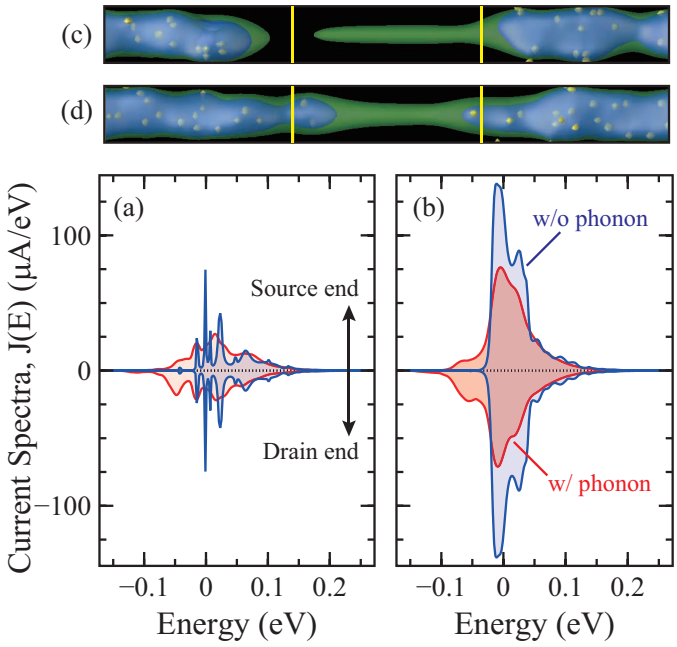

Fig. 6. Current spectra $J_{ph}(E)$ (red) and $J_o(E)$ (blue) for (a) the low-current and (b) the high-current sample at V_d = 0.05 V and V_g = 0.5 V [see arrows in Fig. 5 for the low- and high-current samples]. The corresponding equidensity surfaces are shown in (c) [low-current samples] and (d) [high-current sample]. Blue and greens surfaces correspond to 2×10^{20} and 1×10^{20} cm^{-3}, respectively. Yellow dots represent the dopant locations.

B. Average-Current Reduction

Both the average current, $\langle I\rangle$, and the current fluctuation, σ, become smaller by including phonon scattering. This can be clearly seen in Fig. 4, where the average-current ratio, $\langle I\rangle_{ph}/\langle I\rangle_o$, and the standard deviation ratio, σ_{ph}/σ_o, are plotted as a function of V_g. Here the suffix ph (o) indicates values with (without) phonon scattering. The average-current reduction by phonon scattering, i.e. $1-\langle I\rangle_{ph}/\langle I\rangle_o$, at the off-state ($V_g$ = 0 V) is smaller than that at the on-state (V_g = 0.5 V). This can be attributed to the fact that the phonon-assisted tunneling partially compensates a current loss due to phonon scattering at the off-state [24].

C. Current Fluctuation Suppression

For the current fluctuation, the effect of phonon scattering is significant at higher V_g as shown in Fig. 4(b). For example, $\sigma_{ph}/\sigma_o \approx 0.6$ at V_g = 0.5 V, while $\sigma_{ph}/\sigma_o \approx 0.95$ at V_g = 0.0 V. In order to understand this behavior, we plotted in Fig. 5 the individual current ratio, I_{ph}/I_o, *vs.* I_o. At the off-state [Fig. 5(a) and (b)], I_{ph}/I_o is essentially independent of I_o. The standard deviation ratio, σ_{ph}/σ_o, can, therefore, be considered to be almost equal to the average-current ratio, i.e. $\sigma_{ph}/\sigma_o \approx \langle I\rangle_{ph}/\langle I\rangle_o$. Since the current reduction by phonon scattering becomes smaller at the off-state due to the phonon-assisted tunneling, the reduction in the current fluctuation becomes also small at the off-state. On the other hand, at the on-state [Fig. 5(c) and (d)], there is negative correlation between I_{ph}/I_o and I_o. This suppresses the current fluctuation at the on-state. This negative correlation may be understood by looking at different transport modes between high and low current states (see Fig. 6). For the low-current state, the current spectra, $J_o(E)$, mainly consists of narrow energy windows, which may reflect resonant transmission through localized states. Phonon scattering broadens those narrow energy windows, which enhances the current. On the other hand, for the high-current state, $J_o(E)$ has wider energy windows reflecting band-like transport, and phonons act as normal scattering centers, resulting in the current reduction and leading to the negative correlation.

IV. Conclusion

We investigated the effects of phonon scattering on the RDD-induced current variability in Si NW transistors. We introduced realistic As distributions obtained through the KMC simulation into 10 nm-gate-length n-type GAA Si NW MOSFETs, and calculated the current-voltage characteristics with and without phonon scattering. We find that the current fluctuation is suppressed by ~40 % by phonon scatterings at the on-state, while it is very weakly affected at the off-state. The suppression may be attribute to the different transport modes between high and low current states; i.e. resonant transmission through localized states for lower-current states and band-like transport for higher-current states.

Acknowledgment

We acknowledge Dr. Ignacio Martin Bragado for fruitful discussions on KMC modeling.

References

[1] A. Asenov, "Random dopant induced threshold voltage lowering and fluctuations in sub 0.1 μm MOSFETs: A 3-D 'atomistic' simulation study," IEEE Trans. Electron Devices, vol. 45, pp. 2505-2513, 1998.

[2] S. Roy and A. Asenov, "Where do the dopants go?" Science, vol. 309, pp. 388–390, 2005.

[3] A. Martinez, M. Aldegunde, N. Seoane, A.R. Brown, J.R. Barker, and A. Asenov, "Quantum-transport study on the impact of channel length and cross sections on variability induced by random discrete dopants in narrow gate-all-around silicon nanowire transistors," IEEE Trans. Electron Devices, vol. 58, pp. 2209–2217, 2011.

[4] X. Wang, A. R. Brown, B. Cheng, and A. Asenov, "Statistical variability and reliability in nanoscale FinFETs," 2011 IEEE International Electron Devices Meeting, pp. 103–106, December 2011.

[5] Y. Li, H.-W. Cheng, Y.-Y. Chiu, C.-Y. Yiu, and H.-W. Su, "A unified 3D device simulation of random dopant, interface trap and work function fluctuations on high-κ/metal gate device," 2011 IEEE International Electron Devices Meeting, pp. 107–110, December 2011.

[6] N. Mori, M. Uematsu, H. Minari, G. Mil'nikov, and K.M. Itoh, "Impact of discrete dopant in source and drain extensions on characteristics of nanowire transistors: KMC and NEGF study," 15th International Workshop on Computational Electronics, pp. 105–106, May 2012.

[7] M. Uematsu, K.M. Itoh, G. Mil'nikov, H. Minari, and N. Mori, "Simulation of the effect of arsenic discrete distribution on device characteristics in silicon nanowire transistors," 2012 IEEE International Electron Devices Meeting, pp. 709–712, December 2012.

[8] Sentaurus Process User Guide, Version F-2011.09, Synopsys, Inc. 2011.

[9] M. Uematsu, K.M. Itoh, G. Mil'nikov, H. Minari, and N. Mori, "Discrete distribution of implanted and annealed arsenic atoms in silicon nanowires and its effect on device performance," Nanoscale Res. Lett., vol. 7, pp. 685 (1–6), 2012.

[10] S. Datta, Electronic Transport in Mesoscopic Systems, Cambridge: Cambridge University Press, 1995.

[11] H. Haug and A.-P. Jauho, Quantum Kinetics in Transport and Optics of Semiconductors, Berlin: Springer, 1996.

[12] H. Takeda, N. Mori, and C. Hamaguchi, "Quantum effects on transport characteristics in ultra-small MOSFETs," J. Comput. Electron., vol. 2, pp. 119–122, 2003.

[13] H. Takeda and N. Mori, "Three-dimensional quantum transport simulation of ultra-small FinFETs," J. Comput. Electron., vol. 4, pp. 31–34, 2005.

[14] R. Venugopal, Z. Ren, S. Datta, M.S. Lundstrom, and D. Jovanovic, "Simulating quantum transport in nanoscale transistors: Real versus mode-space approaches," J. Appl. Phys., vol. 92, pp. 3730–3739, 2002.

[15] H. Takeda and N. Mori, "Mode-coupling effects in non-equilibrium Green's function device simulation," Jpn. J. Appl. Phys., vol. 44, pp. 2664–2668, 2005.

[16] V. Eyert, "A comparative study on methods for convergence acceleration of iterative vector sequences," J. Comput. Phys., vol. 124, pp. 271–285, 1996.

[17] A. Pacelli, "Self-consistent solution of the Schrödinger equation in semiconductor devices by implicit iteration," IEEE Trans. Electron Devices, vol. 44, pp. 1169–1171, 1997.

[18] A. Asenov, M. Jaraiz, S. Roy, F. Adamu-Lema, A.R. Brown, V. Moroz, and R. Gafiteanu, "Integrated atomistic process and device simulation of decananometer MOSFETs," International Conference on Simulation of Semiconductor Processes and Devices, pp. 87–90, September 2002.

[19] N. Mori, H. Takeda, H. Minari, "Effects of phonon scattering on electron transport in double-gate MOSFETs," J. Comput. Electron., vol. 7, pp. 268–271, 2008.

[20] C. Jacoboni and L. Reggiani, "The Monte Carlo method for the solution of charge transport in semiconductors with applications to covalent materials," Rev. Mod. Phys. vo. 55, pp. 645–705, 1983.

[21] M. Lundstrom, Fundamentals of Carrier Transport, Cambridge: Cambridge University Press, 2000.

[22] S. Uno, J. Hattori, K. Nakazato, and N. Mori, "Acoustic phonon modulation and electron-phonon interaction in semiconductor slabs and nanowires," J. Comput. Electron., vol. 10, pp. 104–120, 2011.

[23] N. Mori, "Inelastic acoustic phonon scattering in ultra-thin SOI and nanowire structures," 2012 International Conference on Solid State Devices and Materials, E-7-2, September 2012.

[24] H. Takeda and N. Mori, "Effects of electron-phonon interaction on transport characteristics of sub-10-nm bulk-MOSFETs," 2005 International Conference on Solid State Devices and Materials, B-4-1, September 2005.